Reverse blocking enhancement of drain field plate in Schottky-drain AlGaN/GaN high-electron mobility transistors*

Zhao Sheng-Lei(赵胜雷)[a], Wang Yuan(王 媛)[b], Yang Xiao-Lei(杨晓蕾)[b], Lin Zhi-Yu(林志宇)[a], Wang Chong(王 冲)[a], Zhang Jin-Cheng(张进成)[a], Ma Xiao-Hua(马晓华)[a)b], and Hao Yue(郝 跃)[a)†]

[a)] *Key Laboratory of Wide Band-Gap Semiconductor Materials and Devices, School of Microelectronics, Xidian University, Xi'an* 710071, *China*
[b)] *School of Advanced Materials and Nanotechnology, Xidian University, Xi'an 710071, China*

(Received 2 January 2014; revised manuscript received 21 March 2014; published online 16 July 2014)

In this paper, we present the combination of drain field plate (FP) and Schottky drain to improve the reverse blocking capability, and investigate the reverse blocking enhancement of drain FP in Schottky-drain AlGaN/GaN high-electron mobility transistors (HEMTs). Drain FP and gate FP were employed in a two-dimensional simulation to improve the reverse blocking voltage (V_{RB}) and the forward blocking voltage (V_{FB}). The drain-FP length, the gate-FP length and the passivation layer thickness were optimized. V_{RB} and V_{FB} were improved from −67 V and 134 V to −653 V and 868 V respectively after optimization. Simulation results suggest that the combination of drain FP and Schottky drain can enhance the reverse blocking capability significantly.

Keywords: AlGaN/GaN high-electron mobility transistors, reverse blocking capability, drain field plate, Schottky drain

PACS: 73.40.Kp, 73.61.Ey, 78.30.Fs **DOI:** 10.1088/1674-1056/23/9/097305

1. Introduction

Due to high critical breakdown electric field and high two-dimensional electron gas (2DEG) density, AlGaN/GaN high-electron mobility transistors (HEMTs) have been widely investigated as promising candidates for power electronics applications.[1–3] Except for the high forward off-state blocking performance and low specific on-resistance (R_{on}), excellent reverse blocking capability is also desired in a number of applications, such as electric vehicles, class-S amplifiers, and bidirectional switches.[4,5] The drain terminal may be biased at a negative voltage in these applications and this would result in the significant increase of drain current. In previous studies, an AlGaN/GaN HEMT with an integrated recessed Schottky protection diode was fabricated and the reverse blocking capability of this device was better than −110 V.[6]

Various field plates (FPs) were employed in GaN-based HEMTs to improve the forward blocking voltage (V_{FB}), including gate FP, source FP, and slant FP.[7–10] These FPs reduce the electric field at the gate edge and increase the forward blocking voltage significantly. In conventional GaN-based HEMTs, there is no depletion region formed in the vicinity of the drain contact and potential would not concentrate at the drain contact. Hence, drain FP was seldom adopted to improve V_{FB} except for several unconventional GaN-based HEMTs. Resurf AlGaN/GaN HEMT[11] and AlGaN/GaN HEMT with undoped AlGaN layer[12] have an electric field peak at the drain terminal and drain FP is desirable in these HEMTs. For GaN-based HEMT with Schottky drain, Schottky-drain contact depletes the electrons near the drain edge when the drain is reverse biased. Thus, drain FP is necessary in the Schottky-drain AlGaN/GaN HEMTs to be employed to improve reverse blocking capability.

In this paper, the reverse blocking enhancement of the drain field plate (FP) in Schottky-drain AlGaN/GaN high-electron mobility transistors (HEMTs) was investigated by Silvaco-ATLAS. Drain FP and gate FP were employed to improve the reverse blocking voltage (V_{RB}) and V_{FB}. The reverse blocking enhancement of the drain field plate (FP) in Schottky-drain AlGaN/GaN HEMTs has been proposed in a previous work[13] and this paper focuses on the optimization of the drain-FP length, the gate-FP length, and the passivation layer thickness. There can be a very high electric field at the edge of the drain FP or the gate FP, and in-depth discussion about this were carried out to prevent breakdown in the SiN passivation layer.

2. Device structure and simulation model

The simulated Schottky-drain AlGaN/GaN HEMTs utilize a gate FP and a drain FP as shown in Fig. 1. Both the FPs are deposited on a uniform passivation layer ensuring process feasibility. The AlGaN layer under the drain contact is removed and a recessed Schottky-drain HEMT is obtained. Besides the AlGaN layer, the Schottky drain can contact the 2DEG and GaN buffer layer directly to achieve a low onset

*Project supported by the National Natural Science Foundation of China (Grant Nos. 61334002 and 61106106) and the Opening Project of Science and Technology on Reliability Physics and Application Technology of Electronic Component Laboratory, China (Grant No. ZHD201206).

†Corresponding author. E-mail: yhao@xidian.edu.cn

© 2014 Chinese Physical Society and IOP Publishing Ltd

voltage. The Ni metal is utilized to form the gate electrode and Schottky-drain electrode. The HEMT structure includes a 2-μm unintentionally doped (UID) GaN buffer layer above a sapphire substrate, and a 20-nm UID $Al_{0.3}Ga_{0.7}N$ barrier layer. The background doping concentration in GaN and AlGaN layers was assumed to be 1×10^{15} cm^{-3}. The gate length (L_G), the gate–source spacing (L_{GS}) and the gate–drain spacing (L_{GD}) were set to 1 μm, 1 μm, and 10 μm, respectively.

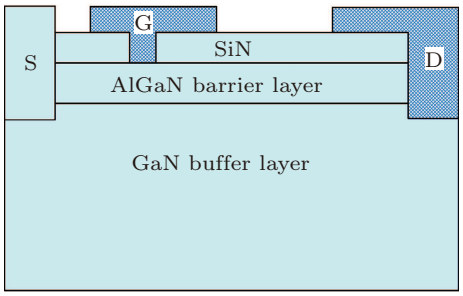


Fig. 1. (color online) Schematic cross section of Schottky-drain AlGaN/GaN HEMT with gate and drain FPs.

The HEMTs were simulated using Silvaco-ATLAS. The positive polarization charge is modeled as a positive fixed sheet charge with a density of 1×10^{13} cm^{-2} along the interface of the heterojunction. The impact ionization is modeled as $\alpha_0 \exp(-E_C/E)$, where $\alpha_0 = 2.9 \times 10^8$ cm^{-1} and $E_C = 3.4 \times 10^7$ V/cm.[14] Using the electron affinity values of 3.8 eV[15] and 1.9 eV[16] for GaN and AlN, respectively, the electron affinity value for $Al_{0.3}Ga_{0.7}N$ was calculated to be 3.23 eV. The V_{FB} and V_{RB} are defined as the drain voltages at which the peak electric field reaches 3 MV/cm.

3. Results and discussion

Figure 2 shows the output characteristics of conventional HEMT and Schottky-drain HEMT. The drain current in the conventional HEMT reaches 457.3 mA/mm with $V_{GS} = 2$ V, and the specific on-resistance R_{on} is 1.53 mΩ·cm^2. The active device areas used in the calculation of R_{on} include a total transfer length of 2 μm for source and drain contacts. In contrast, an onset voltage of 1.0 V (at the drain current of 1 mA/mm) can be observed from the output characteristics of the Schottky-drain HEMT. As a result, the specific on-resistance of the Schottky-drain HEMT is increased to 2.02 mΩ·cm^2. The output characteristics of the AlGaN/GaN HEMTs with gate FP or drain FP are almost the same as that of the AlGaN/GaN HEMTs without FPs.

Figure 3 shows the simulated logarithmic electron concentration in two HEMTs for off-state condition during forward and reverse drain bias. One of the simulated devices is a Schottky-drain HEMT without FPs, the other is a Schottky-drain HEMT with FPs. For the Schottky-drain HEMTs without FPs, the drain metal and the semiconductor materials around it form a Schottky diode. When the drain is reverse biased, strong depletion of electrons in the AlGaN layer and the GaN buffer layer around the Schottky drain electrode can be formed, preventing electrons injecting into the materials, as shown in Fig. 3(a). Thus a good reverse blocking capability was obtained in Schottky-drain HEMT and V_{RB} was −67 V. By using a drain FP, the depletion layer at the drain terminal can be extended, alleviating the electric field concentration at the drain electrode edge, as shown in Fig. 3(b). Simulations indicate that two electric field peaks exist in the HEMT with the drain FP. One peak locates at the edge of the Schottky drain, and the other peak occurs at the edge of the drain FP, as shown in Fig. 4(a). Therefore, the reverse blocking capability can be enhanced by using the drain FP.

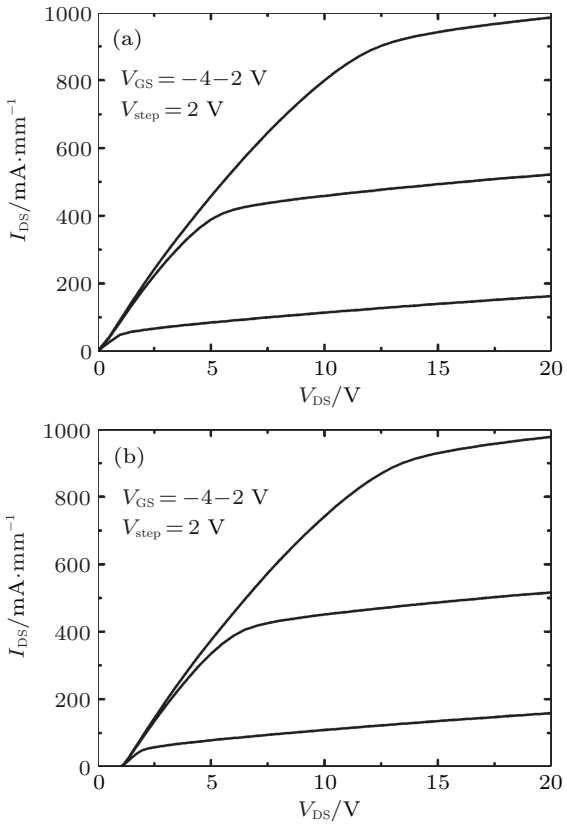


Fig. 2. Output characteristics of (a) conventional HEMT and (b) Schottky-drain HEMT.

When the drain is forward biased, a depletion layer would be formed in the AlGaN layer and the GaN layer around the gate, as shown in Fig. 3(c). There is little depletion layer at the drain terminal formed during forward drain bias, leading to no electric field peak at the drain terminal. For HEMTs without gate FP, the forward blocking voltage was 134 V. The depletion layer at the gate terminal can extend significantly by employing a gate FP, as shown in Fig. 3(d). Two peaks are formed in the electric field distribution, locating at the edge of the gate and gate FP respectively as shown in Fig. 4(b). Thus the forward blocking capability can be improved by employing the gate FP.

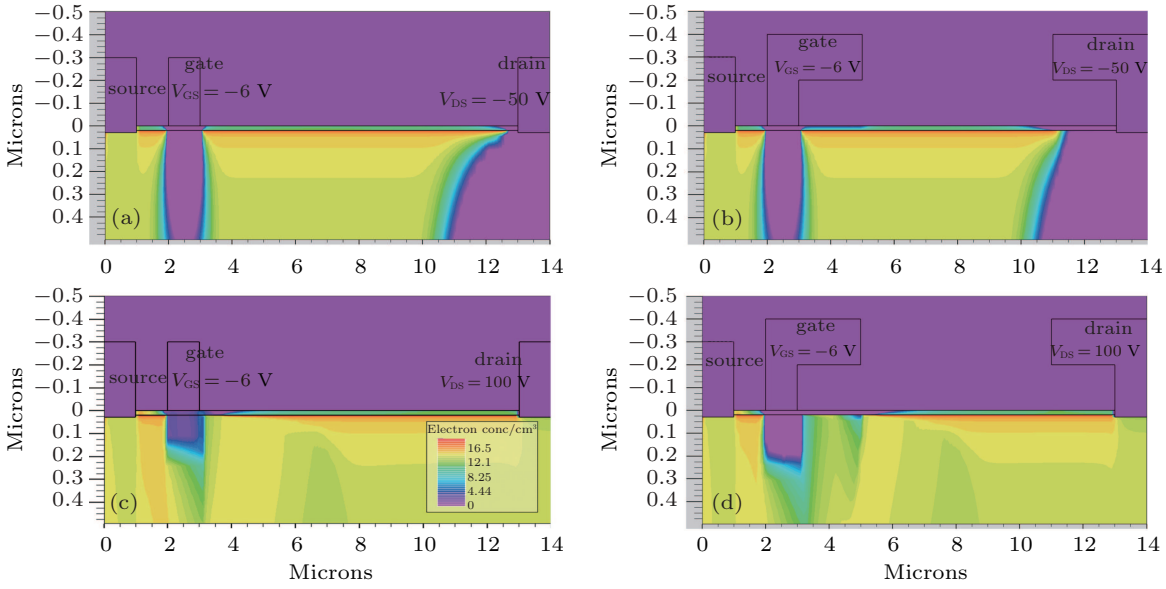


Fig. 3. (color online) Logarithmic electron concentration distribution of the Schottky-drain HEMT (a) without and (b) with FPs in the off state during reverse drain bias, $V_{DS} = -50$ V. Logarithmic electron concentration distribution of the Schottky-drain HEMT (c) without and (d) with FPs in the off state during forward drain bias, $V_{DS} = 100$ V.

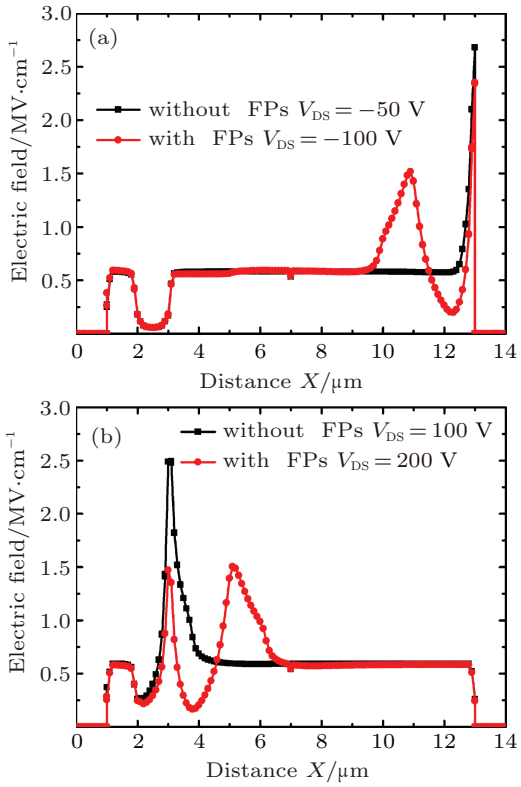


Fig. 4. (color online) Electric field distribution along the AlGaN/GaN interface during (a) reverse drain bias and (b) forward drain bias, $V_{GS} = -6$ V.

Several parameters were optimized to obtain high V_{RB} and V_{FB}, including the drain-FP length, the gate-FP length and the passivation layer thicknesses beneath the two FPs. Both the FPs are deposited on a uniform insulator ensuring process feasibility. The optimization was carried out as follows. The optimum T_{SiN} was obtained from a simulation of V_{RB} as a function of T_{SiN}, keeping L_{DF} and L_{GF} to be 3 μm. For $T_{SiN} = 0$, the electric field at the drain edge is 0 and there is only one peak in the electric field distribution locating at the drain FP edge. With the rise of T_{SiN}, the electric field peak at the drain edge increases and the peak at the drain FP edge decreases. According to the simulation results, the two electric field peaks at the drain edge and the drain FP edge are leveled at $T_{SiN} = 0.24$ μm, and a high V_{RB} of -634 V was achieved. For $T_{SiN} > 0.24$ μm, the peak at the drain edge exceeds the peak at the drain FP edge. As shown in Fig. 5, V_{RB} increases for $T_{SiN} < 0.24$ μm and decreases for $T_{SiN} > 0.24$ μm, indicating the optimum $T_{SiN} = 0.24$ μm. The maximum V_{RB} was obtained from a simulation of V_{RB} as a function of L_{DF}, keeping T_{SiN} to be 0.24 μm. As shown in Fig. 6, V_{RB} increases with L_{DF} for $L_{DF} \leq 2.2$ μm and achieves the maximum $V_{RB} = -653$ V, suggesting the drain FP enhances V_{RB} by about 10 times. For $L_{DF} > 2.2$ μm, the peak at the drain FP edge will exceed the peak at the drain edge, leading to the slight decrease of V_{RB}. In a similar way, the optimum L_{GF} was obtained from a simulation of V_{FB} as a function of L_{GF}, keeping $T_{SiN} = 0.24$ μm. As shown in Fig. 7, the maximum $V_{FB} = 868$ V was achieved for $L_{GF} = 1$ μm.

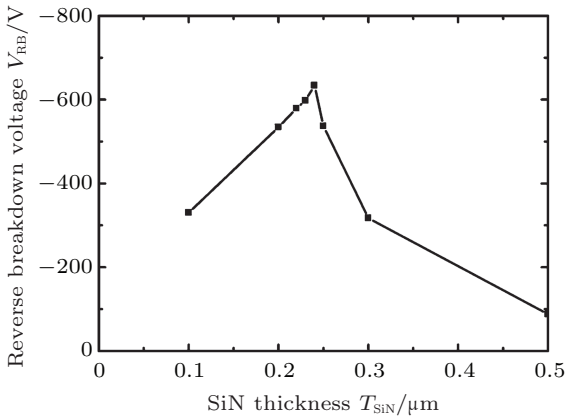


Fig. 5. The V_{RB}–T_{SiN} dependence of the Schottky-drain HEMTs with FPs.

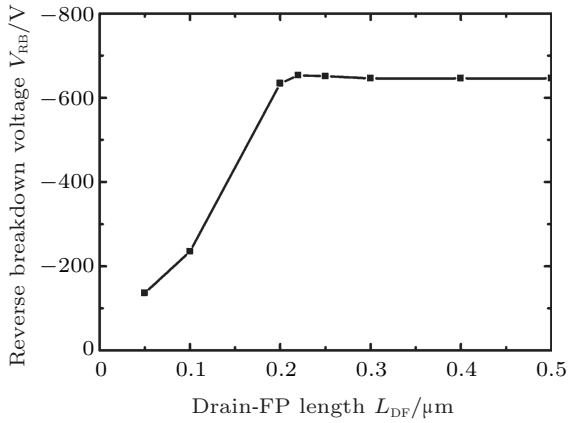


Fig. 6. The V_{RB}–L_{DF} dependence of the Schottky-drain HEMTs with FPs.

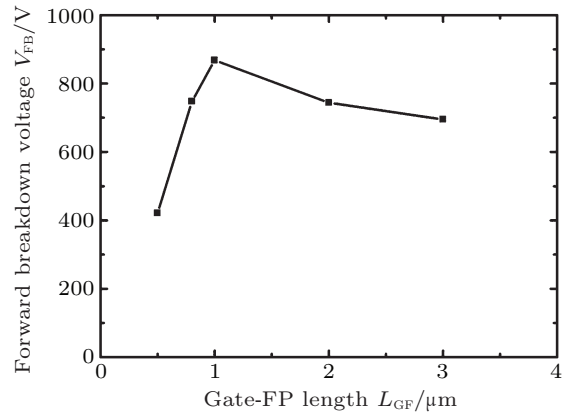


Fig. 7. The V_{FB}–L_{GF} dependence of the Schottky-drain HEMTs with FPs.

The electric fields discussed above are the ones along the AlGaN/GaN heterojunction interface. There can be a very high electric field at the edge of the drain FP or the gate FP and devices may breakdown in the SiN passivation layer first. Thus, it is necessary to discuss the electric field in the SiN film. With $L_{DF} = 2.2$ μm and $L_{GF} = 1$ μm, the distance between the drain FP and the gate FP is 6.8 μm. When the drain is biased at −653 V, the average electric field between the two FPs in the SiN layer is 0.96 MV/cm. The electric field in the SiN layer is nonuniform distributed, and the maximum electric field of 9.1 MV/cm occurs at the drain FP edge. The value of 9.1 MV/cm was achieved at which the peak electric field along the AlGaN/GaN interface reaches 3 MV/cm. If the judging criterion of device breakdown changes from 3 MV/cm to 2 MV/cm or 1.5 MV/cm, the maximum electric field at the drain FP edge would reduce to be 6.8 MV/cm or 5.7 MV/cm. When the drain is biased at 868 V, the average electric field between the two FPs in the SiN layer is 1.28 MV/cm. For the judging criterions of 3 MV/cm, 2 MV/cm, and 1.5 MV/cm, the electric field at the gate FP are 8.6 MV/cm, 6.6 MV/cm, and 5.4 MV/cm, respectively.

The drain-FP length and gate-FP length are optimized from the view point of the optimization of V_{RB}. As a result, the V_{FB} is not the optimal value. In order to achieve the optimal V_{FB} and V_{RB}, the SiN thickness under the two FPs should be designed separately, which will increase the process complexity. Besides, it should be noted that a long drain FP can reduce V_{FB} and a long gate FP can reduce V_{RB} for a certain gate–drain spacing. The distance between the two FPs should be larger than a certain value that can avoid the squeeze of the potential between them.[13] However, the figure-of-merit of power device V_{FB}^2/R_{on} would be reduced by the increased R_{on} for a larger gate-drain spacing L_{GD}. Therefore, it is necessary to consider V_{FB}, V_{RB}, and R_{on} simultaneously and design the device geometry according to the characteristics requirement. For the fabricated ohmic-drain HEMT, the drain and source are ohmic contacts and the deep metallic spikes around the ohmic contact could be formed after high temperature annealing. These deep spikes would cause the electric-field lines to concentrate at the spikes, which may lead to the premature breakdown at the drain terminal. Thus, a drain FP can alleviate the electric field crowding effect in the vicinity of the drain ohmic contact and increase V_{FB}.[17]

The breakdown field of the insulator film strongly depends on the deposition process. The SiN film is generally obtained by a plasma-enhanced chemical vapor-deposition system, and the breakdown field of SiN of 5–10 MV/cm was observed over a wide range of the N/Si ratio.[18] The influence factors of the breakdown field are the vacuum degree, SiH_4/NH_3 flux ratio, temperature, and so on. A high vacuum degree is necessary to reduce impurities in the reaction chamber and improve the purity of the SiN film. The SiH_4/NH_3 flux ratio should be optimized to ensure that the Si/N ratio approaches the stoichiometric value, 0.75.[19] Temperature has an impact on the activities of the atoms and ions decomposed from the two gases, and the value is generally set between 250 °C and 350 °C. The breakdown field of SiN can achieve 12 MV/cm by the optimized process conditions. Besides, He has been proved to be superior to N_2 as a dilution gas and it can improve the properties at decreasing process temperatures. At a temperature of 100 °C, the breakdown field can be enhanced from 4.3 MV/cm to 11.3 MV/cm by using He as a dilution gas.[20]

4. Conclusion

The reverse blocking enhancement of the combination of a drain FP and a Shcottky drain has been investigated in this paper. In two-dimensional simulation, a drain FP and a gate FP were employed to further improve V_{RB} and V_{FB} and the design parameters are the drain-FP length, the gate-FP length and the passivation layer thickness. A drain FP can alleviate the electric field at the edge of the drain electrode, and V_{RB} was improved from −67 V to −653 V by utilizing the drain FP. Simulation results suggest that the combination of drain FP

and Schottky-drain is an effective way to enhance the reverse blocking capability.

References

[1] Shahedipour-Sandvik F, Leathersich J, Tompkins R P, Suvarna P, Tungare M, Walsh T A, Kirchner K W, Zhou S and Jones K A 2013 *Semicond. Sci. Technol.* **28** 074002

[2] Zhao S L, Zhang K, Ha W, Chen Y H, Zhang P, Zhang J C, Ma X H and Hao Y 2013 *Appl. Phys. Lett.* **103** 212106

[3] Tipirneni N, Koudymov A, Adivarahan V, Yang J, Simin G and Khan M A 2006 *IEEE Electron Device Lett.* **27** 716

[4] Huang W and Chow T P 2007 *Proc. ISPSD* p. 265

[5] Morita T, Yanagihara M, Ishida H, Hikita M, Kaibara K, Matsuo H, Uemoto Y, Ueda T, Tanaka T and Ueda D 2007 *IEEE International Electron Devices Meeting*, December 10–12, 2007 Washington, USA, p. 865

[6] Bahat-Treidel E, Lossy R, Würfl J and Tränkle G 2009 *IEEE Electron Device Lett.* **30** 901

[7] Yang L, Hu G Z, Hao Y, Ma X H, Quan S, Yang L Y and Jiang S G 2010 *Chin. Phys. B* **19** 047301

[8] Saito W, Takada Y, Kuraguchi M, Tsuda K, Omura I, Ogura T and Ohashi H 2003 *IEEE Trans. Electron Devices* **50** 2528

[9] Dora Y, Chakraborty A, McCarthy L, Keller S, DenBaars S P and Mishra U K 2006 *IEEE Electron Device Lett.* **27** 713

[10] Zhang K, Cao M Y, Lei X Y, Zhao S L, Yang L Y, Zheng X F, Ma X H and Hao Y 2013 *Chin. Phys. B* **22** 097303

[11] Karmalkar S, Deng J, Shur M S and Gaska R 2001 *IEEE Electron Device Lett.* **22** 373

[12] Saito W, Kuraguchi M, Takada Y, Tsuda K, Omura I and Ogura T 2005 *IEEE Trans. Electron Devices* **52** 106

[13] Zhao S L, Chen W W, Yue T, Wang Y, Luo J, Mao W, Ma X H and Hao Y 2013 *Chin. Phys. B* **22** 117307

[14] Kunihiro K, Kasahara K, Takahashi Y and Ohno Y 1999 *IEEE Electron Device Lett.* **20** 608

[15] Lin S, Kuo C, Liu X, Liang L, Cheng C, Lin C, Tang S, Chang L, Chen C and Gwo S 2012 *Appl. Phys. Express* **5** 031003

[16] Bermudez V M, Wu C I and Kahn A 2001 *J. Appl. Phys.* **89** 1991

[17] Lian Y W, Lin Y S, Lu H C, Huang Y C and Hsu S S H 2012 *IEEE Electron Device Lett.* **33** 973

[18] Fujita S, Ohishi T, Toyoshima H and Sasaki A 1985 *J. Appl. Phys.* **57** 426

[19] Zhou N S, Fujita S and Sasaki A 1985 *J. Electron. Mater.* **14** 55

[20] Arps M and Markwitz A 1997 *J. Vacuum Sci. Technol. A* **15** 1864